Quantitative determination of tip parameters in piezoresponse force microscopy

Sergei V. Kalinin,[a] Stephen Jesse, and Brian J. Rodriguez[b]
Materials Sciences and Technology Division and the Center for Nanophase Materials Sciences, Oak Ridge National Laboratory, Oak Ridge, Tennesse 37831

Eugene A. Eliseev
Institute for Problems of Materials Science, National Academy of Science of Ukraine, 3 Krjijanovskogo, 03142 Kiev, Ukraine

Venkatraman Gopalan
Department of Materials Science and Engineering and Materials Research Institute, Pennsylvania State University, University Park, Pennsylvania 16802

Anna N. Morozovska[c]
V. Lashkaryov Institute of Semiconductor Physics, National Academy of Science of Ukraine, 41, Prospect Nauki, 03028 Kiev, Ukraine

(Received 19 January 2007; accepted 1 May 2007; published online 24 May 2007)

One of the key limiting factors in the quantitative interpretation of piezoresponse force microscopy (PFM) is the lack of knowledge on the effective tip geometry. Here the authors derive analytical expressions for a 180° domain wall profile in PFM for the point charge, sphere plane, and disk electrode models of the tip. An approach for the determination of the effective tip parameters from the wall profile is suggested and illustrated for several ferroelectric materials. The calculated tip parameters can be used self-consistently for the interpretation of PFM resolution and spectroscopy data, i.e., linear imaging processes. © *2007 American Institute of Physics*.
[DOI: 10.1063/1.2742900]

In the last decade, piezoresponse force microscopy (PFM) has emerged as a primary tool for imaging and spectroscopy of ferroelectric materials.[1] Multiple recent applications of PFM include high-resolution imaging of ferroelectric[1] and piezoelectric materials,[2,3] tip-induced polarization switching for data storage[4,5] and ferroelectric lithography,[6] and local hysteresis loop measurements[7,8] and switching spectroscopy mapping.[9] To parallel the spectacular developments in instrumentation, methods, and applications, significant effort has been concentrated on the theoretical description of PFM, including the image formation mechanisms,[10,11] domain wall contrast,[12,13] tip-induced polarization switching,[14–16] and hysteresis loop formation.[9,17] However, all theoretical efforts to date assumed *ad hoc* models for tip geometry, typically using either sphere-plane or point-charge-plane approximations, while the realistic tip geometry is significantly more complex. This lack of knowledge about the tip properties results in large uncertainties in the interpretation of PFM data and precludes reliable quantitative interpretation of switching data, PFM spectroscopy, and domain wall profiles in terms of material parameters. Here, we develop an approach for the determination of the effective parameters of the PFM probe based on the deconvolution of a flat domain wall profile. The determined parameters can be used for the deconvolution of complex domain patterns and spectroscopy data.

The signal in PFM is determined by the convolution of the electric field produced by the tip (probe) with the domain-dependent piezoelectric constant distribution of the material (ideal image). The electric field distribution is determined by the tip geometry and the dielectric properties of the material and the medium. Here, we analyze the case of 180° domain walls in ferroelectrics, corresponding to the most broadly used materials in ferroelectric data storage and lithography applications. In the case of this material symmetry, the dielectric and elastic properties of the material, and hence the tip-induced electric field distribution in the material, do not change across the domain walls.

The analytical approach developed here is based on the decoupled approximation suggested by Felten *et al.*[10] and Scrymgeour and Gopalan[13] and further developed by Kalinin *et al.*[11] Briefly, (a) the electrostatic field is determined from the solution of a rigid dielectric problem, (b) the stress field is calculated using piezoelectric constitutive relations, and (c) the displacement field is calculated for a nonpiezoelectric, elastic material. The uncertainty in this approximation compared to the rigorous solution of the coupled problem is estimated as $s^{-1}_{ijkl}\varepsilon^{-1}_{mp}d_{plk}d_{mrs}$ and is on the order of 2%–20% for most ferroelectric materials. An important consequence of the decoupled approximation is that the experimental PFM image is a linear convolution of the probe function determined by the electric field produced by the tip and the corresponding elastic Green's function, and the ideal image corresponding to a spatial distribution of piezoelectric constants determined by the domain structure of the material. The implications of linearity are analyzed in detail elsewhere.[18] Here, we utilize this approach for calibrating tip properties.

In the case when the electric field produced by the tip does not change across the sample, it is sufficient to determine the effective image charge distribution that represents the tip. Here, we assume that the image charge distribution representing the tip is unknown and is given by the set of N charges Q_i located along the surface normal at distances d_i

[a]Author to whom correspondence should be addressed; electronic mail: sergeiz@ornl.gov
[b]Electronic mail: rodriguezbj@ornl.gov
[c]Electronic mail: morozo@i.com.ua

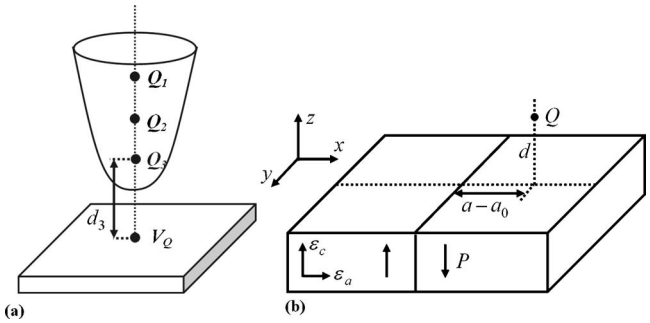

FIG. 1. (a) Representation of a realistic tip by a set of image charges and (b) schematics of the domain wall and single-charge tip.

above the surface, as illustrated in Fig. 1(a). The domain wall profile, i.e., the vertical surface displacement $u_3(a)$ at position a relative to the domain wall at position a_0 produced by a single charge Q at distance d from the surface [Fig. 1(b)] is

$$u_3(s) = \frac{Q}{d}\tilde{u}_3(s) = \frac{1}{2\pi\varepsilon_0(\varepsilon_e+\kappa)}\frac{Q}{d}\{g_{313}(s,\gamma,\nu)d_{31} + g_{351}(s,\gamma)d_{15} + g_{333}(s,\gamma)d_{33}\}, \quad (1)$$

where $s=(a-a_0)/d$ is the coordinate along the domain wall normalized by charge-surface separation, ε_e is the dielectric constant of the medium ($\varepsilon_e=1$ for air and $\varepsilon_e=80$ for water), $\kappa=\sqrt{\varepsilon_{11}\varepsilon_{33}}$ is the effective dielectric constant of material, $\gamma=\sqrt{\varepsilon_{33}/\varepsilon_{11}}$ is dielectric anisotropy factor, and $\nu\approx 0.35$ is Poisson modulus. The functions $g_{ijk}(s,\gamma)$ are

$$g_{351}(s,\gamma) = -\frac{\gamma^2}{(1+\gamma)^2}\frac{s}{|s|+C_{351}(\gamma)}, \quad (2a)$$

$$g_{333}(s,\gamma) = -\frac{1+2\gamma}{(1+\gamma)^2}\frac{s}{|s|+C_{333}(\gamma)}, \quad (2b)$$

$$g_{313}(s,\gamma,\nu) = \frac{1+2\gamma}{(1+\gamma)^2}\frac{s}{|s|+C_{333}(\gamma)} - 2\frac{1+\nu}{1+\gamma}\frac{s}{|s|+C_{313}(\gamma)}. \quad (2c)$$

The constants $C_{ijk}(\gamma)$ depend only on the dielectric anisotropy of the material and, in particular, for $\gamma=1$ the corresponding values are $\{C_{351},C_{333},C_{313}\}=\{0.75,0.25,0.25\}$. For the case of a single point charge, the domain wall profile for $\gamma\approx 1$ can be simplified as

$$d_{33}^{\text{eff}} \approx d_{03} + \left[\frac{3}{4}\left(d_{33}+\left(\frac{1}{3}+\frac{4}{3}\nu\right)d_{31}\right)\frac{s}{|s|+1/4} + \frac{1}{4}d_{15}\frac{s}{|s|+3/4}\right]. \quad (3)$$

Here, we use Eq. (1) to establish an approach for tip calibration in a PFM experiment, i.e., the derivation of the parameters of image charge(s) representing the tip, $\{Q_i,d_i\}_N$, from experimental data.

PFM measurements were performed on a commercial scanning probe microscopy system (Veeco MultiMode NS-IIIA) equipped with additional function generators and lock-in amplifiers (DS 345 and SRS 830, Stanford Research Instruments, and model 7280, Signal Recovery), as described elsewhere.[18] Measurements were performed using Pt and Au coated tips (NSC-12 C, Micromasch, $l=130$ μm, resonant frequency of $\sim$150 kHz, spring constant $k\sim 4.5$ N/m). The samples used were $BaTiO_3$ single crystals, switched domains in $LiNbO_3$, epitaxial lead zirconate titanate (PZT) thin films, and PZT ceramics.

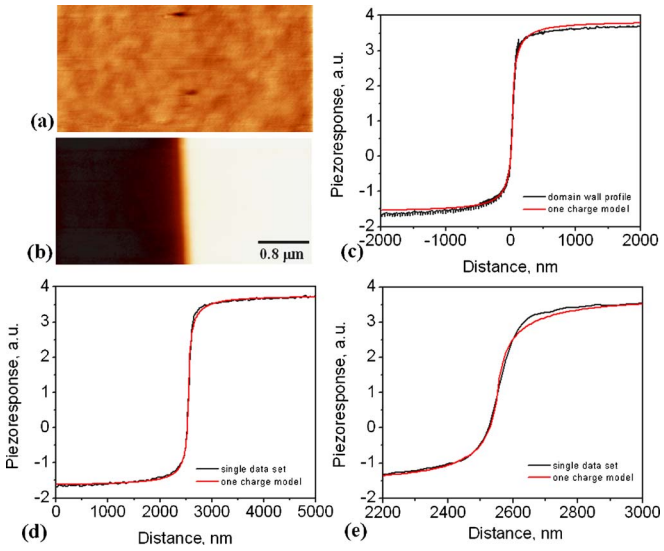

FIG. 2. (Color online) (a) Surface topography and (b) PFM image of a domain wall in $LiNbO_3$. (c) Domain wall profile and corresponding fit by Eq. (4). (d) Fit of the extrapolated data set with equal weighting for all points. (e) Central part of (c) and (d).

The domain wall profile data acquired at multiple scan sizes (i.e., 30 nm, 100 nm, 300 nm, 1 μm, and 3 μm) were exported to ASCII files. To determine tip parameters from experimental data, a MATLAB program was developed. Briefly, the functional

$$F[u_3] = \int\left(PR(a) - \frac{1}{2\pi\varepsilon_0(\varepsilon_e+\kappa)}\sum_{m=0}^{N}\frac{Q_m}{d_m}\tilde{u}_3(s_m)\right)^2 da \quad (4)$$

is minimized with respect to the set of image charges $\{Q_i,d_i\}_N$ representing the tip. Here $PR(a)$ is the measured piezoresponse and integration is performed over all available a values. The number of images charges, N, is predefined. The dielectric constant of the medium can be fixed to the value of free air ($\varepsilon_e=1$) or water in the tip-surface junction or imaging in liquid ($\varepsilon_e=80$). The output of the fitting process is the set of reduced charges $q_i=Q_i/2\pi\varepsilon_0$ and their charge-surface separations d_i. Note that the charges and the dielectric constants cannot be determined independently, since only $Q_m/(\varepsilon_e+\kappa)$ ratios enter Eqs. (1)–(4).

Shown in Fig. 2 is the example of a domain wall profile and the corresponding fit by Eq. (4) with N=1 for $LiNbO_3$. The corresponding image charge parameters are summarized in Table I. Note that while functions in Eq. (1) allow the correct description of the functional behavior of the piezoresponse in the vicinity of the domain wall, the fit quality is significantly reduced for long-distance tails due to different statistical weightings of the regions close to and far away from the center of domain wall. The use of equally spaced data points leads to a better quality fit, as shown in Fig. 2(d). The fit in the vicinity of the domain wall is shown in Fig. 2(e). To improve the fit quality, more complex fitting functions with $N=2$ and $N=3$ were attempted. However, in-

TABLE I. Effective image charge parameters for different ferroelectrics.

			Point charge			Sphere plane (R_0)	
Material	ε_e	Wall width (nm)	Q	d (nm)	Disc R_d (nm)	ε_e=1 (μm)	ε_e=80 (nm)
$LiNbO_3$	1	96	1000	92	58.6	4.8	60
Epitaxial PZT	1	107	2550	125	79.6	5	62.5
PZT in air	1	58	723	86.5	55.1	44	541
PZT in liquid	80	6	104	11.8	7.5	N/A	75

dependent of the choice of the initial values of the image charge, the fit converged to a single image charge, i.e., $d_i=d$ and $\Sigma Q_i=Q$.

Similar behavior was observed for other domain walls studied here, as summarized in Table I. The effective charge-surface separations are compared to the domain wall width determined using a standard Boltzmann fit. Note that for imaging in ambient and using the same tip, the charge-surface separations are comparable. In all cases, only a single image charge can be determined and fits with $N=2$ or 3 result in a convergence of image charges to a single position independently of initial values. Careful inspection of the existing data sets has illustrated that in nearly all cases, the domain wall is asymmetric, i.e., domain wall profiles differ in positive and negative domains. This asymmetry can be due to tip-shape effects and may negatively affect the fitting procedure. To verify this assumption, we attempted fits of a symmetrized domain wall profile, $\tilde{u}_3(a)=(u_3(a-a_0)+u_3(a_0-a))/2$. However, in this case, the single point-charge fit provides a good description of the data as well.

This analysis suggests that the electrostatic field produced by the tip is consistent with a single point charge positioned at a relatively large separation from the surface, contrary to the behavior anticipated in contact mode imaging. To complement the simple point-charge model, we have extended the analysis to the case of a sphere-plane model (radius of curvature R_0) and disk-plane (radius R_d) model. In these cases, the domain wall profile can be approximated by Eq. (1), where effective charge value Q^* and distance d^* are

$$Q^* = \begin{cases} 4\pi\varepsilon_0\varepsilon_e \dfrac{\kappa+\varepsilon_e}{\kappa-\varepsilon_e} \ln\left(\dfrac{\varepsilon_e+\kappa}{2\varepsilon_e}\right) R_0 U, & \text{sphere plane} \\ 4\varepsilon_0(\kappa+\varepsilon_e)R_d U, & \text{disk} \end{cases} \tag{5}$$

and

$$d^* = \begin{cases} \dfrac{2\varepsilon_e}{\kappa-\varepsilon_e} \ln\left(\dfrac{\varepsilon_e+\kappa}{2\varepsilon_e}\right) R_0, & \text{sphere plane} \\ 2R_d/\pi, & \text{disk}. \end{cases} \tag{6}$$

Thus determined parameters are given in Table I. The sphere parameters are calculated both for ambient and water environments to account for possible capillary condensation effects. From the data, it is clear that the use of the sphere/air model leads to implausibly large radii. Hence, experimental data are consistent either with the presence of a capillary water film in the sphere model or conductive disk model. Note that previously developed formalism[14–16] for the polarization switching and spectroscopy in the point-charge model can be directly applied to the sphere model (image charges on one line), but not for the disk model.

To summarize, here we derive a closed-form expression for a domain wall profile in PFM of a 180° domain wall. An approach for determining the effective tip parameters from the wall profile is suggested and illustrated for several ferroelectric materials. Because of the limitations of available experimental data, only the single image charge can be determined reliably, corresponding to sphere/liquid or disk models for the tip. Because of the highly linear behavior of PFM imaging,[18] the calculated image charge parameters can be used self-consistently for the interpretation of PFM resolution and spectroscopic data. Modeling of switching phenomena will require improved estimates of tip geometry.

Research supported by Division of Materials Science and Engineering, Oak Ridge National Laboratory, managed by UT-Battelle, LLC, for the U.S. Department of Energy under Contract No. DE-AC05-00OR22725. VG would like to acknowledge support from NSF-DMR Grant Nos. 0507146, 0512165, 2132623 and 0602986.

[1] *Nanoscale Characterization of Ferroelectric Materials*, edited by M. Alexe and A. Gruverman, (Springer New York, 2004)..
[2] B. J. Rodriguez, A. Gruverman, A. I. Kingon, R. J. Nemanich, and O. Ambacher, Appl. Phys. Lett. **80**, 4166 (2002).
[3] S. V. Kalinin, B. J. Rodriguez, S. Jesse, T. Thundat, and A. Gruverman, Appl. Phys. Lett. **87**, 053901 (2005).
[4] H. Shin, S. Hong, J. Moon, and J. U. Jeon, Ultramicroscopy **91**, 103 (2002).
[5] T. Tybell, P. Paruch, T. Giamarchi, and J.-M. Triscone, Phys. Rev. Lett. **89**, 097601 (2002).
[6] S. V. Kalinin, D. A. Bonnell, T. Alvarez, X. Lei, Z. Hu, and J. H. Ferris, Adv. Mater. (Weinheim, Ger.) **16**, 795 (2004).
[7] A. Roelofs, U. Böttger, R. Waser, F. Schlaphof, S. Trogisch, and L. M. Eng., Appl. Phys. Lett. **77**, 3444 (2000).
[8] H. Y. Guo, J. B. Xu, I. H. Wilson, Z. Xie, E. Z. Luo, S. Hong, and H. Yan, Appl. Phys. Lett. **81**, 715 (2002).
[9] S. Jesse, B. Mirman, and S. V. Kalinin, Appl. Phys. Lett. **89**, 022906 (2006).
[10] F. Felten, G. A. Schneider, J. Muñoz Saldaña, and S. V. Kalinin, J. Appl. Phys. **96**, 563 (2004).
[11] S. V. Kalinin, E. A. Eliseev, and A. N. Morozovska, Appl. Phys. Lett. **88**, 232904 (2006).
[12] C. S. Ganpule, V. Nagarjan, H. Li, A. S. Ogale, D. E. Steinhauer, S. Aggarwal, E. Williams, R. Ramesh, and P. De Wolf, Appl. Phys. Lett. **77**, 292 (2000).
[13] D. A. Scrymgeour and V. Gopalan, Phys. Rev. B **72**, 024103 (2005).
[14] M. Molotskii, J. Appl. Phys. **93**, 6234 (2003).
[15] A. N. Morozovska and E. A. Eliseev, Phys. Rev. B **B**, 73, 104440 (2006).
[16] A. Yu. Emelyanov, Phys. Rev. B **B**, 71, 132102 (2005).
[17] A. Wu, P. M. Vilarinho, V. V. Shvartsman, G. Suchaneck, and A. L. Kholkin, Nanotechnology **16**, 2587 (2005).
[18] S. V. Kalinin, S. Jesse, B. J. Rodriguez, J. Shin, A. P. Baddorf, H. N. Lee, A. Borisevich, and S. J. Pennycook, Nanotechnology **17**, 3400 (2006).